

Crystalline topological defects within response theory

Sami Hakani* and Itamar Kimchi†

School of Physics, Georgia Institute of Technology, Atlanta, GA 30332

(Dated: October 31, 2023)

Lattice defects have interesting effects in some quantum Hamiltonians. Here we show how topological crystalline defects can produce qualitatively new effects by coupling to electric field probes such as Raman scattering, even when they do not appear in the low-energy Hamiltonian but rather only in the probe response theory. To show this we consider an antiferromagnetic spin-1/2 model H_{spin} on a zigzag chain. Crystalline domain walls between two zigzag domains appear as at most local defects in H_{spin} , but as topological (not locally creatable) defects in the Raman operator R of inelastic photon scattering. Using TEBD numerics, bosonization, and mean field, we show that a finite density of crystalline domain walls shifts the entire Raman signal to produce an effective gap. This lattice-defect-induced Raman gap closes and reopens in applied magnetic fields. We discuss the effect in terms of photons sensing the lattice defects within R as spin-dimerization domain walls, with Z_2 character, and a resulting shift of the probed wavevector from $q = 0$ to $\pi + \delta q$, giving an $O(1)$ change in contrast to local defects. The magneto-Raman singularity from topological lattice defects here relies on the H_{spin} spinon liquid state, suggesting future applications using lattice topological defects to modify response-theory operators independently of H and thereby generate new probes of quantum phases.

I. INTRODUCTION

Crystalline defects are increasingly understood to offer useful probes of quantum phases of matter. For example, weak 3D topological insulators host a 1D topological modes in dislocation lines [1]; spin-1/2 two leg ladders show singlet breaking with few percent impurities [2]; defects in quantum spin liquids host low energy modes [3, 4]. In these and many other examples, crystal or lattice defects probe a quantum phase by modifying the wavefunction in particular ways. Here we describe how in certain scenarios crystal defects can qualitatively change the result of experiments that involve photons or electric fields by coupling directly to the electric fields and thereby modifying the probe theory operator, independently of whether or not the defects modify the original system's Hamiltonian.

In particular we require *topological* crystalline defects. For concreteness we focus on crystalline domain walls of the two zigzag/zag-zig domains of a zigzag chain (a.k.a. sawtooth chain with mirror symmetries) of a spin-1/2 antiferromagnet. Such defects may appear in the spin Hamiltonian, but if so, only as local defects (i.e. locally creatable, in contrast to topological defects which are not locally creatable). In contrast they can appear in electric field probes, such as the Raman operator of inelastic photon scattering, as true topological defects. As we discuss below, this allows the topological crystalline defects to shift the effective wavevector probed by the photons in a manner related to the defect concentration, resulting in an additional contribution in the probe operator that is $O(1)$ for any defect concentration. This $O(1)$ effect should be contrasted with the effect of local defects,

which for defect concentration ϵ is only $O(\epsilon)$. This is the case even when local defects give qualitatively new features, as when locally reduced symmetry near a defect allows transitions from previously-forbidden matrix elements [5]; these transitions appear with amplitude ϵ . The $O(1)$ effects seen here, occurring in a bulk probe even at small defect concentrations, rely on each defect modifying the probe operator on infinitely many sites, and hence require the crystalline defects to be non-locally-creatable i.e. topological.

Below we show that the Raman operator for a zigzag domain has explicit spin dimerization; and moreover, zigzag domain walls manifest as dimerization domain walls. It is interesting to consider what such dimerization domain walls would do if they appeared in a Hamiltonian. Previous studies have shown that dimerization domain walls carry a spin-1/2 degree of freedom for protected “topological” reasons associated with the quantum anomaly of a single spin-half, with similar effects occurring in 2D frustrated magnets [6]. Given that dimerization domain walls in a Hamiltonian carry such topologically-protected spin-1/2 modes that respond to magnetic fields, it is interesting to study the dimerization domain walls in the Raman operator, induced by crystal defects, and ask whether they too have a magnetic response. Surprisingly, below we show that non-magnetic crystal defects indeed do give rise to a magnetic response within Raman scattering.

If they are found in experiments on a new unstudied material, the surprising effects we predict – such as a Raman gap closing and reopening with applied magnetic fields – could easily be misinterpreted. They could naively be thought to arise as an intrinsic magnetic signature of some phase, or as effects from magnetic impurities. The framework we present is necessary for a correct interpretation; in this case, as effects from non-magnetic crystal defects combined with 1D-fractionalized spinon

* shakani3@gatech.edu

† ikimchi3@gatech.edu

excitations.

Our main purpose in this work is to argue for the general effect of crystalline topological defects modifying response theory operators, and to present a proof-of-principle toy model. This toy model however may still adequately describe some magnetic insulator compounds. Let us suggest some materials. $\text{Rb}_2\text{Cu}_2\text{Mo}_3\text{O}_{12}$ is a zigzag spin-half chain compound with a singlet ground state and large couplings (ferromagnetic $J_1 \approx -138$ K and antiferromagnetic $J_2 \approx 51$ K); a Luttinger Liquid phase may arise in a small applied field [7, 8]. AgCrP_2S_6 is a zigzag chain compound where Kramer’s doublet spin-3/2 magnetic sites interact with a nearest neighbor antiferromagnetic exchange of order 100 K [9, 10]. Copper benzoate [11] is a spin-1/2 antiferromagnetic chain compound; the Cu-Cu bonds do not zigzag, but the oxygen octahedra coordinating Cu have alternating orientations on successive Cu sites, so that the symmetry is equivalent to a zigzag chain. Coupling of the lattice to electric fields will generate topological defects in the Raman operator in exchange paths above lowest order, i.e. beyond the Loudon-Fleury approximation [12], for example through Cu-O superexchange, which gives the Cu-O vector dotted with photon polarization. (The magnetic field should be applied in a direction that avoids generating an effective staggered field [13].) In all these materials, one limiting factor may be the Raman resolution at low frequencies, which must be high enough to resolve effects at frequencies set by typical inverse domain sizes. Nevertheless here resolving low frequency features is helped by the strong inelastic signal at $\omega \rightarrow 0$, which is not present in typical $q = 0$ Raman experiments.

The remainder of this paper is structured as follows. In Section II we present the model (Fig. 1) and discuss its Raman response including in the presence of crystalline domain walls, through the coupling between crystalline domains and photon polarizations (electric fields). For each domain the Raman operator R is a *dimerization* operator which breaks the translation symmetry of the spin Hamiltonian H . This is in contrast with spin-Peierls (dimerized or valence bond solid) materials such as CuGeO_3 , where R and H are both explicitly dimerized [14]. When Hamiltonians or wavefunctions show explicit dimerization, it is well known that dimerization domain walls carry protected spin-1/2 modes with a strong magnetic signal [6]. Surprisingly, here dimerization domain walls in the Raman operator, created by crystalline domain walls, also produce a magnetic signal. Using TEBD (time evolving block decimation) numerics, bosonization, and mean field, we find that a density of domain walls creates a gap in the Raman spectrum. This gap closes and then reopens above a critical magnetic field set by the typical domain size. We explain the effects in terms of a shift of the wavevector probed by the photon scattering, from $q = 0$ typical in solid state Raman to $q = \pi$ for a single domain, to $q = \pi + \delta q$ with multiple domains of typical size $\pi/\delta q$, combined with the magnetic field response of the fermionic excitations in the gapless Lut-

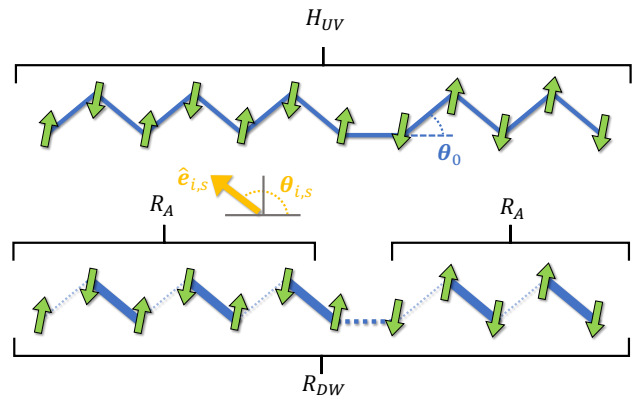


FIG. 1. (Top) The lattice-level Hamiltonian H_{UV} for a spin-1/2 zigzag chain contains information on spatial positions. This information may be invisible to the low energy spin Hamiltonian H_0 (Eqn. 3) since H_0 has identical antiferromagnetic couplings on “zig” and “zag” bonds. (Bottom) Inelastic Raman scattering probes the the Raman operator R dynamical correlations within H_0 . However R knows about H_{UV} spatial positions through the photon electric fields. For some photon polarizations $\hat{\mathbf{e}}_i, \hat{\mathbf{e}}_s$ (especially diagonal or cross polarizations so $\theta_i + \theta_s = \pi/2$), the Raman operator is an alternating dimerization operator R_A (Eqn. 6). Zigzag domain walls in H_{UV} , separating the two zigzag domains, do not appear as topological defects within H_0 . However within R they manifest and become dimerization domain walls, separating two distinct R_A dimerization domains. Thus R_{DW} contains a topological defect.

tinger liquid phase of a spin-1/2 antiferromagnetic chain.

In Section III we discuss these results, their restrictions and generalizations. That these features arise from domain walls rather than local defects is also seen in a Z_2 characteristic that we discuss, wherein two defects brought close together have no anomalous response. We discuss the effects of local defects on the 1D spin Hamiltonian, which are known to be RG-relevant in 1D, resulting in a distribution of finite size chain fragments, whose finite size gaps closely mirror the results in the limit discussed above. For both of these limits (unperturbed and fixed-point-fragmented Hamiltonian) we discuss the distribution of domain sizes and its effects on the expected features. Finally we show that the effects here arise from domain walls probing the fermionic spinon excitations, by computing the domain wall Raman response for other candidate phases – ferromagnets, antiferromagnets, and gapped phases of integer spin chains such as the AKLT phase – and show that the features described above rely on the gapless spinon phase. Thus the features can also be interpreted as a modification of Raman scattering, via crystalline domain walls, in order to probe the 1D-fractionalized spinon excitations.

II. RESULTS

A. Introduction to Raman Scattering

The inelastic Raman scattering spectrum $I(\omega)$ of a system is specified by its Hamiltonian H , the ground state, and a third ingredient, the Raman operator R . This third ingredient is needed to describe the photon-in-photon-out scattering process; the wavevector of the photons is sufficiently small that it can be ignored, but photon frequency and polarizations remain important. In terms of R , the spectrum $I(\omega)$ is computed as the dynamical correlation function,

$$I(\omega) = \frac{1}{2\pi} \int_{-\infty}^{\infty} dt e^{i\omega t} \langle R(t)R(0) \rangle_0 \quad (1)$$

Here we work at zero temperature so $\langle \cdots \rangle_0$ is the ground state expectation value, easily modified for finite temperature. The key player here is the Raman operator R , which includes information on the photon polarizations and associated electric fields. In the simplest limit applicable to a spin model, the so-called Loudon-Fleury (photon-induced superexchange) form of the operator [15] is

$$R = \sum_{\mathbf{r}_1, \mathbf{r}_2} (\hat{\mathbf{e}}_i \cdot \mathbf{r}_{12})(\hat{\mathbf{e}}_s \cdot \mathbf{r}_{12}) A(\mathbf{r}_{12}) \mathbf{S}_{r_1} \cdot \mathbf{S}_{r_2} \quad (2)$$

In Eq. (2), $\hat{\mathbf{e}}_{i(s)}$ is the incident (scattered) photon polarization and $\mathbf{r}_{12} = \mathbf{r}_1 - \mathbf{r}_2$. Ratios of $A(\mathbf{r}_{12})$ on different bonds are of the order of the ratio of the respective exchange couplings, since they are similarly generated by superexchange. Moreover, from the definitions above it is evident that two Raman operators R and R' yield the same inelastic scattering spectrum under a Hamiltonian H if there exists a real constant c such that $R' = R - cH$, since cH does not time evolve. A pair of R and R' differing by a multiple of H are spectrally equivalent.

Since photon polarizations ($\hat{\mathbf{e}}_{i,s}$) necessarily couple to spatial degrees of freedom (\mathbf{r}_{12}), the Raman operator inherits a rich structure from the spatial geometry of the system, endowing R with symmetries that are different from the symmetries of the Hamiltonian H (Fig. 1).

B. Raman Response of the Clean Zigzag Chain

We begin by computing the Raman operator and Raman response for a 1D spin-1/2 zigzag chain in the clean limit, with a single domain. Here we will consider an effective 1D antiferromagnetic spin-1/2 zigzag chain in the presence of an applied magnetic field in order to highlight the interplay between spatial geometry, Raman operator structure, and the associated Raman response. Importantly, within a single zigzag domain, the spin Hamiltonian H_{spin} for this system is blind to the zigzagging. For simplicity we focus on nearest neighbor couplings and

take H_{spin} to be a standard 1D antiferromagnetic XXZ spin chain given by

$$H_0 = J \sum_j (\mathbf{S}_j \cdot \mathbf{S}_{j+1} + (\Delta-1)S_j^z S_{j+1}^z) - h^z \sum_j S_j^z \quad (3)$$

with $J > 0$, and where the H_0 subscript refers to the clean limit. Although the ultraviolet Hamiltonian for a spin-1/2 zigzag chain contains information about both spin and lattice degrees of freedom, at low energies the infrared Hamiltonian is an effective 1D spin-1/2 XXZ chain as depicted in Fig. 1. For the remainder of this section, we take the magnetic field $h^z = 0$; magnetic field effects will be considered further below.

The zigzag spin chain geometry and Eq. (2) give the following form for the Raman operator when $\Delta = 1$:

$$R \propto \sum_j [f_{\theta_i, \theta_s, \theta_0} + h_{\theta_i, \theta_s, \theta_0} (-1)^j] (\mathbf{S}_j \cdot \mathbf{S}_{j+1}) \quad (4)$$

where $\theta_{i,s}$ is the angle of the incident/scattered photon polarization (measured from the zigzag chain axis), θ_0 is the zigzag angle (Fig. 1), $f_{\theta_i, \theta_s, \theta_0} = \cos \theta_i \cos \theta_s \cos^2 \theta_0 + \sin \theta_i \sin \theta_s \sin^2 \theta_0$, and

$$h_{\theta_i, \theta_s, \theta_0} = \frac{1}{2} \sin(2\theta_0) \sin(\theta_i + \theta_s). \quad (5)$$

When $\theta_i + \theta_s = \frac{\pi}{2}$, the alternating part of R is maximized. Physically, this alternating part is maximized, relative to any other terms which can arise for generic Hamiltonians, for the physically relevant cases of: cross polarizations ($\theta_i = 0, \theta_s = \frac{\pi}{2}$; or vice versa); and parallel polarizations along a diagonal ($\theta_i = \theta_s = \frac{\pi}{4}$).

When the alternating part of R is considered, the Raman operator for this system has a dimerization structure and is given by

$$R_A \propto \sum_j (1 + (-1)^j) (\mathbf{S}_j \cdot \mathbf{S}_{j+1}) \quad (6)$$

where we recall that Raman operators R and R' are spectrally equivalent if they differ by a multiple of H . Unlike the spin Hamiltonian which has discrete translational invariance by one lattice site, R_A explicitly breaks this translational invariance. In particular R_A generally also has lower symmetry than the full Hamiltonian of the material: for example, the zigzag chain of Fig. 1 has mirror symmetry across each site, while R_A does not. Its symmetry is reduced through the coupling of the crystal lattice with photon polarizations or electric fields.

While typically a Raman response in solids does not give a gapless inelastic ($\omega \approx 0$) response, here at $T = 0$ we capture a gapless inelastic Raman response due to the alternating structure of R_A induced by the zigzag geometry. The lowest order nonvanishing contribution to the Raman response at the mean field level (see below and Appendix B) is given by

$$I(\omega) \propto \sqrt{1 - \left(\frac{\omega}{2v_s} \right)^2} \quad (7)$$

This continuum is computed at mean field as a 2-particle response. The low energy effective field theory also predicts a gapless inelastic response for $0 \leq \Delta < 1$ [16]. We note, however, at the $SU(2)$ symmetric point ($\Delta = 1$) bosonization (see below) gives a purely elastic response: $I(\omega) \rightarrow \delta(\omega)$. Nonetheless, away from that point, both mean field and bosonization capture a gapless inelastic Raman response for R_A due to its alternating structure.

C. Raman Response of Zigzag Chains with Zigzag Domain Walls

We now turn to Raman scattering in the presence of crystalline topological defects, here zigzag domain walls i.e. multiple zigzag domains. Although zigzag domain walls modify the Hamiltonian of the system by acting as a local (not topological) defect, and similarly the local defect part of the domain wall (e.g. the horizontal bond) can appear in R_{DW} in a non-universal manner, we address these modifications later and find they do not qualitatively change our conclusions. For now, let us suppose zigzag domain walls only alter the Raman operator, and only by altering each domain.

1. Numerics (DMRG and TEBD)

Using a combination of density matrix renormalization group (DMRG) and time evolving block decimation (TEBD), we numerically compute the $T = 0$ inelastic Raman scattering spectra as a function of frequency and applied magnetic field, for both zero domain walls and two domain walls (Fig. 2). We use spin chains of length $L=80$ with open boundary conditions.

Our numerics for the zero domain wall case show a prominent low energy excitation at a frequency ω^* . In applied field h^z , we find ω^* shifts to higher frequencies linearly with h^z . The finite gap at low frequencies can be attributed to the finite size of the system. Indeed we find $(\omega^*/J) \sim L^{-1}$ as the system size is increased.

The two domain wall case shows a zero field gap that is larger than the finite size gap of the zero domain wall case. Moreover, for small applied fields the gap shrinks to the finite size gap of ω^* . At larger fields, the gap increases.

2. Mean field theory

To understand these numerical results, let us discuss the results from a mean field computation of the effects of domain walls on R . For $\Delta = 0$, the Hamiltonian is an XY model and the mean field mapping is exact with Jordan-Wigner fermions. Within mean field, the Hamiltonian is a spinon Fermi sea $H_0^{MF} = \sum_k \epsilon_k c_k^\dagger c_k$ with spinon field operators defined by $\{c_k, c_{k'}^\dagger\} = \delta_{kk'}$, dispersion $\epsilon_k = -v_s \cos(k)$, and spinon velocity v_s , with $v_s = J$ at $\Delta = 0$

(we take unit lattice spacing throughout). In mean field, the Raman operator R_q is a spinon density excitation

$$R_q = \sum_k V_{kq} c_k^\dagger c_{k-q} \quad (8)$$

where the vertex is $V_{kq} = \frac{1}{2}(e^{i(k-q)} + e^{-ik} - 1 - e^{-iq})$. (Details are below and in Appendix B and C.) Note that nonzero Δ adds interactions and also modifies the bandwidth; at $\Delta = 1$, the spinon velocity is given by $v_s = \frac{\pi}{2}J$ as determined by the exact Bethe ansatz result for this system [17].

While clean zigzag chains show a gapless Raman response (Eq. (7)), we find that when there are multiple zigzag domains, and hence multiple domains of R_A (Eq. (6)), the Raman response becomes gapped. The gap occurs at a frequency ω_c where $\omega_c = v_s(\pi/L_d)$ where L_d is the size of the domain between the two domain walls (unit lattice spacing) and v_s is the spinon velocity. Here we consider domains of a particular size; the generalization to a distribution of domain sizes is discussed below. The presence of the gap in the 2-particle continuum may be surprising since in computing the scattering spectrum, neither the Hamiltonian nor the ground state are altered. Indeed, the only difference between these responses is the presence of zigzag domain walls.

In applied field, we find another surprising result: at a small finite fields the gap closes then reopens (Fig. 3, top row). With L_d the domain size, the gap in the Raman spectrum closes at a small applied field of $h_c = \frac{1}{2}v_s(\pi/L_d)$ and reopens for $h^z > h_c$. We again emphasize that in this case, the Hamiltonian is blind to the presence of the zigzag domain walls. Moreover the domain walls are non-magnetic defects, and naively one would not expect such a drastically different response in the presence of applied magnetic field.

3. Bosonization

In the clean zigzag chain, we previously stated that the mean field spectrum at the 2-particle level did not even qualitatively capture the delta function response computed using bosonization. This inconsistency begs the question as to whether these results of a singular magnetic field response domain walls are robust beyond mean field. We find that they are.

At low frequencies the Raman response can be described analytically via bosonization of the interacting spinon model. (For details such as discussion of renormalization of Luttinger parameter K with magnetic field, see Appendix D.) At the 2-particle level for R (though Hamiltonian interactions are captured by K) we use the density-density response function computed in bosonization. Linearizing momenta about the Fermi points of the spinon liquid, we find the vertex contribution V_{kq} is constant. Hence the 2-particle Raman response of R_q reduces to density-density correlation function within

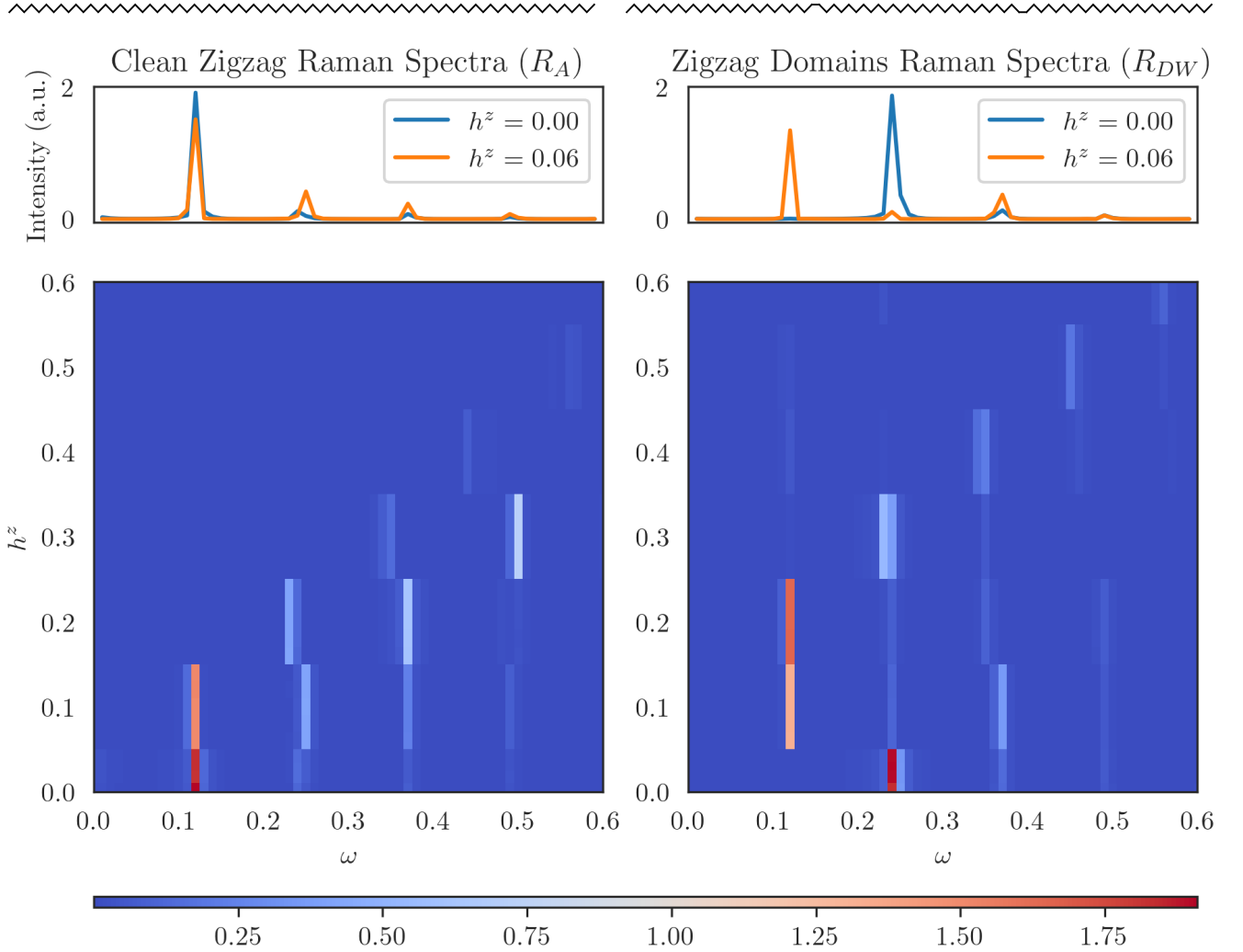


FIG. 2. (Top) Inelastic magneto-Raman spectra as a function of frequency ω and applied magnetic field h^z , computed numerically using DMRG and TEBD for a finite size $L=80$ Heisenberg spin-1/2 chain ($J=1, \Delta=1$, open boundaries). Left column: clean system with single R_A domain; right column: three R_A domains in the R_{DW} Raman operator, separated by two domain walls (at $j_1=26$ and $j_2=54$, giving domain size $L_d=27$). In both cases the Hamiltonian H_0 is identical; the only difference is in the Raman operator. The line drawing of the corresponding H_{UV} zigzag chain is shown at top. Upper panel: line cuts of spectra at zero and nonzero fields show that while the clean R_A is independent of small fields, the domain walls of R_{DW} show a singular response to magnetic fields. Lower panel: color plots of spectra as function of magnetic field show the full behavior. At zero field, the presence of domain walls shifts the finite size gap to higher energy. This shift persists up to a small critical field; the critical field value is consistent with the theoretical expectation $h_c = \frac{1}{2}v_s(\pi/L_d)$ with $v_s = \pi/2$. Spectral weight shifts upward with field above $h^z = 0$ for zero defects and above $h^z = h_c$ for two defects.

bosonization up to an arbitrary scale factor. This correlation function is given by [18]

$$\chi_{\rho\rho}(q, \omega) \propto -\frac{\sin(\pi K)}{v_s} \left(\frac{2\pi}{\beta v_s} \right)^{2K-2} F(v_s, q, \omega) \quad (9)$$

with

$$F(v_s, q, \omega) = \prod_{\eta=\pm 1} B\left(-i\frac{\beta(\omega + \eta v_s q)}{4\pi} + \frac{K}{2}, 1-K\right) \quad (10)$$

and $B(x, y)$ Euler's beta function. The Raman response of R_q is then $-\text{Im}(\chi_{\rho\rho}(q, \omega))$.

Though interactions beyond mean field do have an important qualitative effect, and though $SU(2)$ symmetry at the two-particle level of the bosonization computation is again qualitatively distinct, nevertheless the bosonization results, Fig. 3, qualitatively match our numerically generated Raman spectra (Fig. 2).

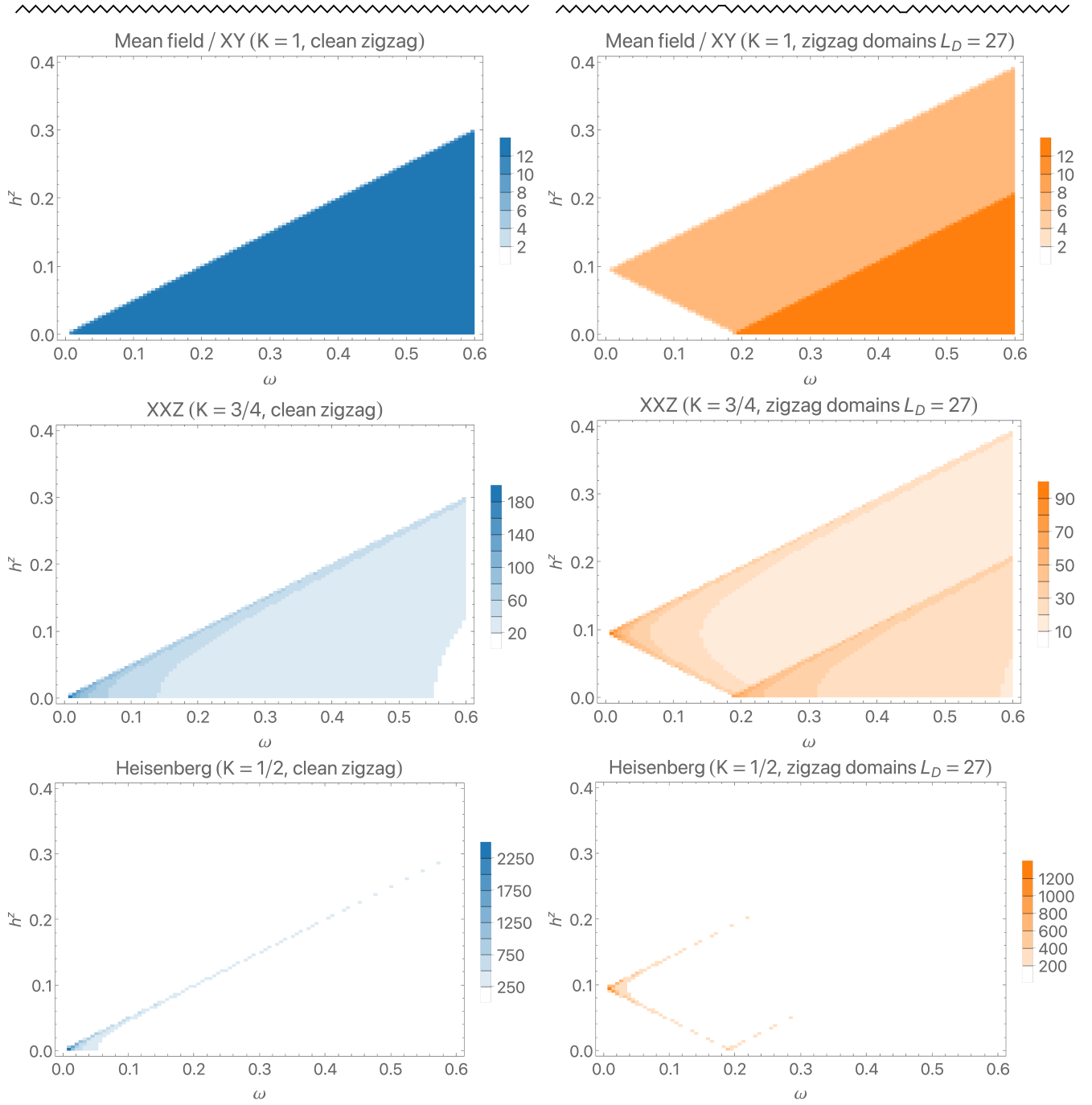


FIG. 3. Low frequency magneto-Raman spectra computed via field theory bosonization (Eq. (D2)), for the clean zigzag chain R_A (left column, blue) versus the R_{DW} chain with multiple zigzag domains (of size $L_d=27$) (right column, orange). For ease of comparison, spinon velocity is fixed as $v_s = \pi/2$. Top row: XY model, $\Delta = 0$, where mean field is exact (Luttinger parameter $K = 1$). Middle: a representative XXZ response for intermediate Δ (at $K = 3/4$). Bottom: The $\Delta = 1$ SU(2) Heisenberg Hamiltonian ($K = 1/2$), with a delta function singularity. Across the interaction range, the clean zigzag spectra shows gapless excitations whose gap increases linearly with applied magnetic field. In the presence of zigzag domain walls, a Raman gap is opened, but closes and then reopens with applied magnetic field.

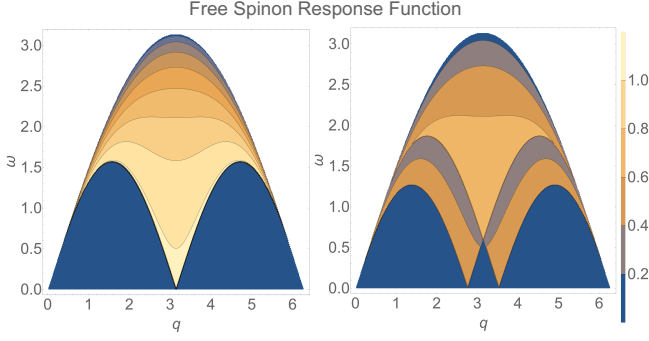


FIG. 4. $\chi(q, \omega)$ two-fermion response function for a mean field free spinon Hamiltonian with $v_s = \pi/2$, at zero field (left) and small applied field $h^z = 0.3$ (right). At this level the Raman spectrum is a weighted sum over $\chi(q)$ given by Eq. (15). For a clean zigzag chain, it is just a cut through χ at $q = \pi$. In the presence of zigzag domain walls, the Raman spectrum contains cuts at Fourier modes of the domain profile, $q \neq \pi$; for domains of typical size L_d , the most significant contributions come from $q = \pi \pm \pi/L_d$.

D. $O(1)$ changes via wavevector shifts

In the previous sections, we described our results that non-magnetic crystal defects (zigzag domain walls) in a spin chain give a singular magnetic field response as measured by inelastic Raman scattering. This effect is not only captured in mean field, but it is also reproducible numerically (via TEBD) and analytically (at low energies using bosonization) in the presence of strong interactions. In this section, we describe the mean field (and associated setup for bosonization) analysis in detail, to explain how non-magnetic crystal defects induce a singular magnetic field response. These computational details will anchor the discussions in the following section.

We capture the effects of defects in the Raman operator by considering the Raman response of a sum of Heisenberg terms R_j with coefficients g_j :

$$R = \sum_j g_j R_j, \quad R_j \equiv \mathbf{S}_j \cdot \mathbf{S}_{j+1} \quad (11)$$

where the couplings g_j are specified by the photon polarization factor of equation Eq. (2). We will call g_j the bond profile of the Raman operator.

By Fourier transforming g_j , the operator R can be rewritten as a weighted sum over its Fourier modes as

$$R = \sum_q \tilde{g}_q R_q, \quad R_q = \sum_j e^{iqj} (\mathbf{S}_j \cdot \mathbf{S}_{j+1}) \quad (12)$$

where \tilde{g}_q are the Fourier modes of g . The Raman response of a generic Raman operator R is then given by

$$I(\omega) = \sum_{qq'} \tilde{g}_q \tilde{g}_{q'} \int dt e^{i\omega t} \langle R_q(t) R_{q'}(0) \rangle_0 \quad (13)$$

We now compute the correlation function $\langle R_q(t) R_{q'}(0) \rangle_0$. This object is only nonzero for $q + q' = 0$, and so it suffices to compute $\langle R_q(t) R_{-q}(0) \rangle_0$. We then define the Fourier transform of this correlation function to be

$$\chi(q, \omega) = \int dt e^{i\omega t} \langle R_q(t) R_{-q}(0) \rangle_0 \quad (14)$$

so that the Raman intensity of R is given by

$$I(\omega) = \sum_q |\tilde{g}_q|^2 \chi(q, \omega) \quad (15)$$

Raman spectra are a weighted sum over finite q probes depending on the functional form of g . Even when photons carry effectively zero momentum, Raman is not always a $q = 0$ probe.

The response χ is easily understood in mean field. We use the Jordan-Wigner transformation to map spin operators to spinless fermionic operators and compute the response χ to lowest nonvanishing order in fermionic operators (Appendix B). At this order, χ is a response function involving 4 fermion operators, given by $\chi^{MF}(q, \omega)$,

$$\chi^{MF} = \sum_{k_0} \frac{8}{2\pi} \frac{\sqrt{(2v_s \sin(q/2))^2 - \omega^2}}{(2v_s \sin(q/2))^2} f(k_0)(1 - f(k_0 - q)) \quad (16)$$

where f is the Fermi function, $\epsilon_k = -v_s \cos k$, and k_0 are the wavevectors that satisfy energy conservation $\omega + \epsilon_{k_0} - \epsilon_{k_0 - q} = 0$; at low frequencies, $k_0 = \pm 2k_F$ (where the Fermi wavevector is $k_F = \pi/2$ at zero magnetic field). At low frequencies the relevant part of χ is just this $2k_F$ response,

$$\chi(q, \omega) \sim \sum_{\pm} \Theta(\omega - v|q \pm 2k_F|) \quad (17)$$

with Θ the Heaviside step function. We plot χ^{MF} in Fig. 4.

Raman scattering of a clean zigzag spin chain with zero domain walls is a $q = \pi$ probe. Here $R_A \propto \sum_j (-1)^j \mathbf{S}_j \cdot \mathbf{S}_{j+1}$ with bond profile $g_j = (-1)^j$, giving a Fourier transform of $\tilde{g}_q \propto \delta_{q, \pi}$. Using Eq. (16) at zero magnetic field and at $q = 2k_F = \pi$, where χ is gapless, we find the gapless response $I(\omega) \propto \sqrt{1 - (\omega/2v_s)^2}$.

Zigzag domain walls create a zero-field gapped response because the Raman scattering probe for the spin chain is shifted away from $q = \pi$. The amounts of the shift across various wavevectors is given by the Fourier transform power spectrum of the bond profile; if domains have a typical size L_d , this Fourier transform will be sharply peaked at $\pi \pm \pi/L_d$. For large L_d , the zero-field gap is $\omega_c \approx v_s \delta q = v_s(\pi/L_d)$. This gap closes and then reopens in applied magnetic field because the Fermi momentum k_F of the fermionic spinons changes in applied field. The magnetic field is the chemical potential of spinons. In the presence of zigzag domain walls, the Raman spectrum as probing excitations at q away from

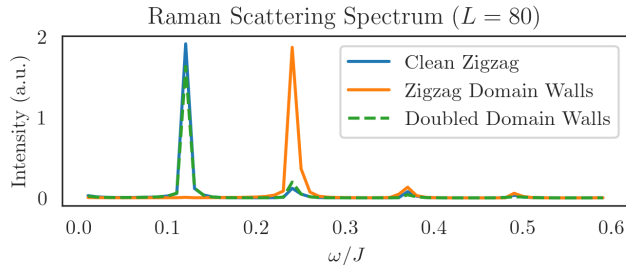


FIG. 5. Inelastic Raman spectra computed with DMRG and TEBD for a finite size $L=80$ Heisenberg spin-1/2 chain with zero domain walls (solid, blue), two domain walls (solid, orange), and doubled domain walls (dashed, green). The two domain wall system is the same as shown in the right-hand column of Fig. 2. The doubled domain wall system has two domain walls on sites $j_1=39$ and $j_2=41$. The three systems have the same Hamiltonian, and only vary in the choice of Raman operator. For doubled domain walls, the zero magnetic field gap associated with the presence of isolated domain walls is no longer observed, showing that the effect of domain walls arises from their Z_2 character as topological defects, rather than from local defect effects.

π . In applied field, however, k_F also shifts from π such that the finite momentum probed by Raman scattering can be in resonance with the new Fermi momentum (i.e. $q \pm \delta q = 2k_F$). Hence the gap closes in applied fields. At larger magnetic fields $2k_F$ shifts further and the gap reopens.

III. GENERALIZATIONS AND DISCUSSION

A. Z_2 Characteristic and other distinctions between topological defects and local defects

Domain walls are topological defects in that to create them one must create an entire domain. This nonlocality enables them to produce an $O(1)$ change in the response theory. Associated with that nonlocality, domain walls also have a Z_2 character. This Z_2 character is indeed seen in the response to such defects: when the spatial separation between domain walls becomes small, the anomalous magnetic field response is no longer observed in our numerics (Fig. 5). In contrast, local (non-topological, or, geometric) defects don't show a Z_2 character and only add a small additive component to the response. We now discuss these two distinctions in detail.

Isolated domain wall defects shift the probed wavevector. For a single domain, the wavevector probed in the Raman response is $q = \pi$. The presence of a topological defect in the form of a zigzag domain wall causes the Raman response to shift from $q = \pi$ to $q = \pi + \delta q$. The length of zigzag domains L_d fixes the small wavevector $\delta q = \pi/L_d$. Put another way, the Raman operator for the system changes from R_A (or $R_{q=\pi}$) to $R_{\pi \pm \delta q}$. The subsequent Raman response changes from

$$\chi(q = \pi, \omega) \rightarrow \chi(q = \pi + \delta q, \omega).$$

Doubled (nearby) domain walls are a local defect. They are locally creatable, and thus do not change the wavevector probed by the clean system, and instead only add a small amplitude component on top of the clean system response. In terms of wavevectors, the doubled domain wall is local in real space and hence spread widely in reciprocal space, mostly on large wavevectors Q whose response $\chi(Q, \omega)$ vanishes at low frequencies. The crossover from the topological nature of well separated domain walls to local nature of two domain walls in close proximity to each other can also be seen numerically (Fig. 5).

Another example of local (non-topological) defects is a small amplitude variation in the zigzag angle θ_0 for the spin chain. It does not shift the wavevector probed in Raman scattering for the clean system. Suppose θ_j is the bond angle on the j th bond, and we let $\theta_j = \theta_0 + \epsilon f_j$ for a mean angle of θ_0 , a small amplitude ϵ , and an arbitrary function of position f_j . In this case, we have (Eq. (G12))

$$I(\omega) = A\chi(\pi, \omega) + \epsilon^2 \cos(2\theta_0) \sum_q |\tilde{f}_q| \chi(q + \pi, \omega) \quad (18)$$

where A is $O(1)$. Here, the Raman response is composed of the clean system response at $q = \pi$ and a small $O(\epsilon^2)$ component. Whereas topological defects shift the Raman response to $q \neq \pi$, geometric defects only add a small component rather than shifting the wavevector probed.

B. Role of Average Symmetry

We note that the disordered system with domain walls still has an average symmetry which is key to the observations described above. On average, neither domain is preferred over the other. This average symmetry ensures that the domains occur with equal probability, and hence that the $q = 0$ component of the domain structure Fourier transform vanishes exactly. This ensures that the distribution of δq has no weight at $q = 0$ and hence no gapless response remains in the Raman response at zero field.

A related feature is that the average symmetry ensures exact cancellation of the contribution of each single domain. Writing the Raman operator R as a sum over domain D_1 and domain D_2 terms R_1, R_2 , the dynamical R correlation function clearly contains a direct term of $R_1 R_1$ and $R_2 R_2$, which at zero field produce a gapless response. What happens to that gapless response? The answer is that it is exactly cancelled out by the cross terms $R_1 R_2$. This exact cancellation requires the average symmetry.

C. Effect of Zigzag Domain Walls as local defects within the Hamiltonian

Above we consider the effects of domain walls purely in modifying the domains in the Raman operator, in order to isolate the effects of crystalline topological defects within a response theory. However in addition to this effect, the domain wall does create a local defect both in R and in H . We now discuss these local effects. In the particular 1D model considered here, perturbations to the Hamiltonian are easily RG-relevant due to the 1D physics, so we will also discuss the resulting effects in a 1D chain, noting however that local defects will not have such strong effects in 2D or 3D systems.

Microscopically it is clear that local defect effects arise at domain walls. Modifications in the Hamiltonian would arise from changes in the spin exchange coupling due to any changes in the bond length. The relative orientation of these bonds with photon polarizations would also affect their bond strength in the Raman operator.

In 1D, local bond perturbations to the Hamiltonian are relevant in the renormalization group (RG) sense [19]. The fixed point of the RG flow breaks apart the system into two open chains. For a weak bond, the end points of the chain are precisely the two adjacent lattice sites between which the exchange coupling is reduced; for a strong bond, a singlet is formed, but the chain is cut away from this singlet.

When zigzag domain walls are present in spin chains and modify the Hamiltonian locally, the RG fixed point of the system is a set of fragmented finite size chains of varying length given by the size of each zigzag domain. Finite chains of length L_d have a true finite size gap, hence a gapped Raman response, associated with the finite size wavevector $q = \pi \pm \pi/L_d$. Magnetic fields tune the chemical potential through these finite sized wavevectors. Thus in both the limit where the Hamiltonian breaks apart into fragmented chains and in the limit where it does not (and e.g. is unmodified), the presence of zigzag domain walls gives a Raman response at a finite wavevector away from the wavevector probed by the clean system.

Above we have also computed the Raman spectra numerically in finite size systems. This corresponds to an intermediate case, where the Hamiltonian perturbation is included, but the fixed point of fragmented chains is not yet reached. This can occur physically if the RG flow is arrested by some effective finite size effects, e.g. a moderately weak bond from a domain wall where the next domain walls have already completed an RG flow to decoupling, such that the domain wall occurs within a finite chain fragment. Numerically for $L = 80$ sites, the Raman spectra are quite similar to those of an unperturbed Hamiltonian. We also look at varying the strength of the horizontal domain wall bond within R , which can vary corresponding to the strength of the corresponding bond in H , in a manner that also depends on photon polarizations. The results are again qualitatively independent of this modification (see Fig. 8).

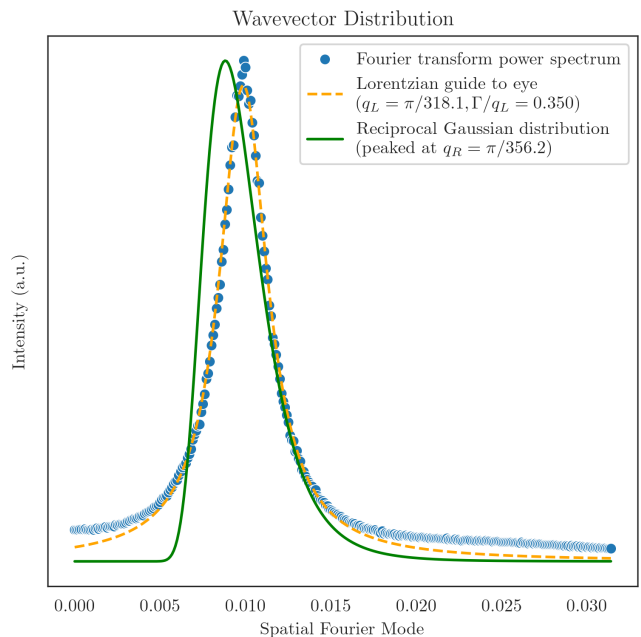


FIG. 6. Distributions of wavevector deviations from π that are relevant for zigzag domains whose sizes follow a Gaussian distribution with mean $\mu = 300$ and standard deviation $\sigma = 100$. Blue circles: numerically averaged power spectrum of Raman operator bond profile (10^3 chains of length 10^5), giving the wavevector distribution in the unmodified Hamiltonian limit. Orange dashed: Lorentzian centered at q_L with FWHM Γ as a guide to the eye. Green solid: reciprocal Gaussian distribution, giving finite size gaps in the fragmented chain segments limit.

We next turn to comparing the two distributions of wavevectors in both the unperturbed and perturbed H limits.

D. Distribution of Domain Sizes

The above sections considered the case of a particular size of zigzag domains. Here we consider the realistic case of a distribution of domain sizes. The crystalline domain size is expected to be a random distribution with a typical length scale set by the competition between the cost of domain walls and the preference to have a single domain. For example, this can be modeled in an equilibrium approximation by considering a random “field” that locally prefers one of the two crystalline domains. The resulting Imry-Ma mechanism [20] for discrete order in 1D gives domains at the Larkin length. Indeed generally for disordered elastic media subjected to random fields (such as a local preference for one crystalline domain), the disorder seen by domain walls has long range correlations even when the microscopic disorder is short ranged correlated.

To model a typical length scale arising from various equilibrium and nonequilibrium mechanisms, we consider

a Gaussian distribution of domain lengths with mean μ and variance σ^2 . In the limit where domain walls don't substantially modify the Hamiltonian, the resulting Raman spectra are set by integrating over wavevectors weighted by the Fourier transform power spectrum of the bond profile of the Raman operator (Eq. (H3)). Numerically computing the power spectrum we find it to be approximately a Lorentzian centered at $q_L \approx \pi/\mu$. In the fixed point limit where the Hamiltonian is strongly modified by the domain walls, the system becomes an ensemble of fragmented spin chains each with their own finite size gaps. These finite size gaps follow a reciprocal Gaussian distribution, peaked at $q_R = \pi(-\mu + \sqrt{\mu^2 + 8\sigma^2})/(4\sigma^2)$. As a general statement for the mean of the reciprocal distribution independent of the L_d distribution, note that the wavevector shift is $dq = \pi/L_d$ for each chain fragment of size L_d , so its expectation value is bounded from below by π/L_d by Jensen's inequality: $\overline{dq} > \pi/\overline{L_d}$, as indeed seen for the reciprocal Gaussian. Both distributions (Fig. 6) are sharply peaked, resulting in magneto-Raman spectra with a soft gap but still showing the features described above (Fig. 7).

The importance of the long range effects that set a typical domain size can be seen by considering an opposite limit, where every site has an independent probability of hosting a domain wall. The resulting distribution of domain sizes is Poisson. This is unphysical: crystalline domains would not form a Poisson distribution, since for example it would be energetically preferred to shift two nearby domain walls together and annihilate them at the small cost of flipping an unfavored domain. A Poisson distribution would however be expected for locations of non-topological local defects with no associated domains. Such a Poisson distribution ("random telegraph signal") would produce a $q = 0$ centered Lorentzian power spectrum. It would show a gapless Raman signal at nonzero fields, but would not show the singular gap behavior of domains with typical length scale.

E. Topological Defects Here Probe Spinon Liquid Physics

The singular magnetic field responses of zigzag domain walls described above were computed within the Luttinger Liquid ground state of H_0 . Here we show that they rely on the special properties of this gapless spinon phase, and in particular that they are absent in systems with ferromagnetic order, antiferromagnetic order, and in the gapped AKLT phases.

To study these phases we compute the response of the operator R_q from equation Eq. (11) within linear spin-wave theory (LSWT) to compute a 4-magnon response function analogous to equation Eq. (14). It is well known [21], however, that quantum fluctuations in 1D diverge and obstruct magnetic order. Nonetheless, we employ LSWT in order to gain intuition for how quasi-1D spin chains may behave in the presence of magnetic order me-

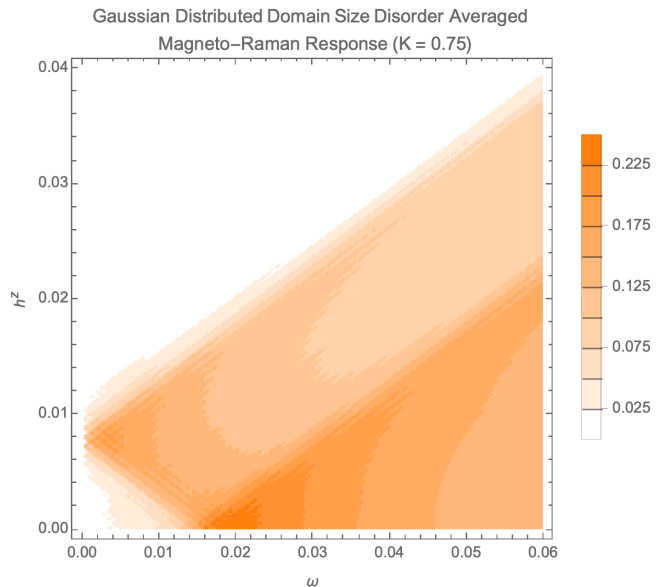


FIG. 7. Magneto-Raman spectrum for zigzag domains of R_{DW} with a distribution as in Fig. 6, with Luttinger parameter $K = 3/4$ and spinon velocity $v_s = \pi/2$.

diated by interactions in 3D.

Whereas an applied magnetic field shifts the Fermi momentum of a spinon Fermi surface, and may tune gapped excitations to become gapless, bosonic magnon excitations do not experience such an effect. Indeed, for 1D magnons we find no similar anomalous magnetic field response that is probed by Raman scattering. We first consider magnons in a ferromagnetic phase in applied magnetic field. Next, we consider the antiferromagnetic phase at zero applied field. In this case, we find the Raman response to be non-vanishing at the 2-magnon level. In applied field, however, the classical ground state of the antiferromagnet changes. At finite field, the Raman response then becomes non-vanishing at the 1-magnon level and qualitatively follows the dynamical structure factor probed by neutron scattering. Finally we consider the gapped AKLT phase. In all cases, however, the magnetic field dependence of the Raman response lacks the anomalous response we find for free spinons in the main text.

1. Comparison with Ferromagnetic Order

In a ferromagnet, low temperature excitations away from the classically ordered ground state are magnons with bosonic particle statistics. Following a similar approach with our spinon mean field analysis, we compute $\chi^{FM}(q, \omega)$ with a magnon parton construction within linear spin wave theory. In this approximation, the ground state is the magnon vacuum. The Raman operator R_q , however, is a magnon density excitations at finite q . Explicitly we find $R_q = \sum_k \Gamma_{kq} a_k^\dagger a_{k+q}$ where the vertex

$\Gamma_{kq} = S(e^{-i(k+q)} + e^{ik} - (1 + e^{-iq}))$. Since R_q annihilates the ground state, the $T = 0$ Raman scattering spectrum within linear spin wave theory vanishes at zero field. Although applied magnetic fields open a gap in the single particle spectrum, the classical ground state remains unchanged. As such zigzag domain walls have no anomalous magnetic field response as in the case of the spinon liquid.

2. Comparison with Antiferromagnetic order

Zigzag domain walls also have no anomalous magnetic field response for the spin- S antiferromagnetic Heisenberg Hamiltonian in the ordered phase. Whereas the inelastic Raman scattering spectrum vanishes in the ferromagnetic phase, it does not vanish in the presence of antiferromagnetic order. The Raman response of antiferromagnetic magnons qualitatively follows the single magnon dispersion analogous to the spin dynamical structure factor measured in neutron scattering experiments. Unlike the ferromagnetic phase, where the Raman operator R_q is a magnon density excitation, in the antiferromagnetic phase we find the lowest order contribution to the Raman operator is a single magnon excitation (Appendix F 2). As such, the lowest order contribution to the Raman response $\chi^{AFM}(q, \omega)$ qualitatively follows the single magnon dispersion. A significant difference from the neutron scattering analogy, however, is that the Raman response χ has a relative π shift in momentum. This momentum shift carries from the π wavevector associated with the classical Néel ordered ground state from which spins cant in applied magnetic field.

For sparse domain wall densities, the Raman response is peaked at $q = \pi \pm \delta q$ with δq small. Moreover, the Response follows the single magnon dispersion with a relative π shift in momentum. Antiferromagnetic magnons at $q = \pi$ are gapless, and in applied field they remain gapless. Excitations near $q = \pi$ always remain gapped. Moreover, since magnons are bosonic and have no Fermi momentum, applied fields cannot close the gap opened by the presence of domain walls. Consequently, although domain walls open a gap in the spectrum, this gap would not close in the presence of an applied field.

3. Comparison with AKLT phase

Zigzag domain walls in the AKLT phase again do not have a singular low energy magnetic field response as above, as can be simply seen by their gap. The integer spin 1D Heisenberg antiferromagnetic in applied field has the Hamiltonian $H = J \sum_j \mathbf{S}_j \cdot \mathbf{S}_{j+1} - h^z \sum_j S_j^z$. At zero field, the system has a gapped singlet ground state. The gap $\Delta \approx 0.41J$ for $S = 1$ [22]. This gap closes for $h > \Delta$ at which the system experiences magnon condensation [23]. For the Luttinger liquid phase the presence of crys-

tal domain walls induces a gap $(\omega^*/J) \sim 1/L \ll \Delta$ in the Raman response. The gap closes for small magnetic fields $h^z > \omega^*$. Since the AKLT chain remains gapped for fields below Δ , we do not expect such a nontrivial magnetic field response for small magnetic fields.

IV. OUTLOOK

In this work we argued that in certain settings, crystalline topological defects can modify the response of an electronic system not just by changing the electronic state, but also by changing the response theory operator. In particular this arises in experiments that involve electric fields or photon scattering. We presented a proof-of-principle toy model using Raman scattering on a zigzag spin half chain with zigzag crystalline domain walls. In this toy model, even in the limit where domain walls only enter the Raman operator and not the Hamiltonian, still they produce singular effects in the Raman spectra, including singularities in applied magnetic fields. Such effects may be otherwise unexpected from nonmagnetic crystal disorder.

One way to understand the response is as arising from an effective shift of the wavevector probed by the Raman scattering (which is conventionally at $q = 0$). Intriguingly, this wavevector shift arises from dimerization domain walls, which are here only within the Raman operator; in contrast dimerization domain walls in a spin-half Hamiltonian carry spin-half modes protected by the spin half quantum anomaly. Is there also an aspect of the Raman response here that is associated with a quantum anomaly? The Raman operator is not a Hamiltonian, so the framework needed to answer this question does not exist. However even though Raman is a scattering experiment, i.e. its theory is not a conventional linear or perturbative response theory, it could be considered to be a linear response theory with a contrived probe function which is the Raman operator. Nonlinear responses at zero frequency then involve this operator being added to the Hamiltonian. The resulting modified Hamiltonian would then carry explicit dimerization, and domain walls of this dimerization could carry anomaly-protected spin-half modes. Any such effects would necessarily be non perturbative. Could there be such quantum anomaly features associated with response theory operators? We leave this question for future work.

Other future avenues should explore the modification of response theories in higher spatial dimensions, and in particular as a way to modulate experimental response operators to tailor them as probes of particular otherwise-hard-to-probe quantum entangled phases. Already even simple Raman spectroscopy has been shown to be a useful probe of quantum spin liquid phases [24–26]. The ability to modify the effective wavevector probed, or make further modifications with real space resolution, just by adding crystalline topological defects, could be of much help. Importantly, crystalline topo-

logical defects may be a mild type of disorder for some quantum states and hence such defects can be added even intentionally, without destroying the desired quantum state. In this way the addition of crystalline topological defect can serve as a way to tune experimental response theory probes while preserving the quantum state.

ACKNOWLEDGEMENTS

The authors acknowledge helpful discussions with Ehud Altman, Erez Berg, Natalia Drichko, Zhigang Jiang, Yuan-Ming Lu, Martin Mourigal, Tyrel McQueen, Colin Parker, Natasha Perkins, Daniel Podolsky, Hide Takagi, Achim Rosch, and Masaki Oshikawa. This work was supported in part by the National Science Foundation under Grants No. NSF PHY-1748958 and PHY-2309135. This work was also performed in part at the Aspen Center for Physics, which is supported by National Science Foundation grant PHY-1607611.

APPENDIX

Appendix A: Numerical Details

Numerical simulations of Raman spectra were performed using the TeNPy library [27]. The ground state $|\psi\rangle$ is computed using DMRG (density-matrix renormalization group), initialized as a matrix-product state with Néel order. The Hamiltonian H and Raman operator R for a given simulation are written as matrix-product operators. To compute the Raman intensity, we compute the correlation function $\langle\psi|R(t)R(0)|\psi\rangle$ and Fourier transform to the frequency domain. Magnetic field values were taken in steps of 0.1, and additional steps of 0.02 at small fields (below 0.2 for the main text figures, below 0.1 for the appendix figures).

To compute $\langle\psi|R(t)R(0)|\psi\rangle$, we compute the equivalent quantity $e^{i\epsilon_0 t} \langle\psi|R|\phi(t)\rangle$, where ϵ_0 is the ground-state energy, $|\phi(0)\rangle = R|\psi\rangle$, and $|\phi(t)\rangle = e^{-iHt}|\phi\rangle = e^{-iHt}R|\psi\rangle$. DMRG produces both $|\psi\rangle$ and ϵ_0 , and time-evolution of $|\phi\rangle$ is performed using time evolving block decimation (TEBD). This procedure requires only one instance of DMRG and TEBD to be performed to compute the correlation function and thus reduces the time needed to perform the simulation.

The ground state of a finite size ($N = 80$) open $S = 1/2$ chain was found using DMRG with 10^{-10} precision in the ground state energy ϵ_0 . Bond dimension of 100 was found to be enough for convergence. Singular values were truncated below 10^{-10} .

TEBD was performed using time step of $\Delta t = 0.0628$ at Suzuki-Trotter order 4 with a built-in optimization described in [28]. Numerical time evolution was performed for 10^5 time steps. Bond dimension of 100 was again found to be enough for convergence. (recall we are computing time evolution with a local Hamiltonian starting from a ground state, so entanglement growth is

relatively weak.) Singular values were truncated below 10^{-12} . These parameters were chosen to obtain a frequency resolution $\Delta\omega \approx 0.01$ and reduce Trotterization error.

Appendix B: Mean Field Theory

In the main text we compute Raman responses using a mean field treatment. In this section for completeness we walk an interested reader through how to do the mean field computation. Within mean field, we take the Hamiltonian to be a free spinon theory given by

$$H = \sum_k \epsilon_k c_k^\dagger c_k, \quad \epsilon_k = -v_s \cos k \quad (\text{B1})$$

with spinon operators obtained via a Jordan-Wigner transformation and, for Heisenberg Hamiltonian, the dispersion bandwidth set to the Bethe ansatz results for the spinon dispersion [17]. For the Raman operator $R_q = \sum_j e^{iqj} (\mathbf{S}_j \cdot \mathbf{S}_{j+1})$ we then seek to compute the dynamical correlation function $\langle R_q(t) R_q(0) \rangle_0$ on the ground state.

To lowest order in fermionic operators, the inelastic part of the Raman operator R_q in terms of Jordan-Wigner spinons is given by

$$R_q = \sum_k V_{kq} c_k^\dagger c_{k-q} \quad (\text{B2})$$

with the vertex given by

$$V_{kq} = \frac{1}{2} (e^{i(k-q)} + e^{-ik} - 1 - e^{-iq}) \quad (\text{B3})$$

The Raman operator R_q is a spinon density excitation at momentum q . At time t , the operator R_q is given by

$$R_q(t) = \sum_k e^{i(\epsilon_k - \epsilon_{k-q})t} V_{kq} c_k^\dagger c_{k-q} \quad (\text{B4})$$

The desired dynamical correlation function $\langle R_q(t) R_q(0) \rangle_0$ can then be written as

$$\sum_{kk'} e^{i(\epsilon_k - \epsilon_{k-q})t} V_{kq} V_{k'q'} \langle (c_k^\dagger c_{k-q})(c_{k'}^\dagger c_{k'-q'}) \rangle_0 \quad (\text{B5})$$

where the first two fermionic operators are time ordered before the latter two. We evaluate this expression using Wick's theorem which only gives the following inelastic diagrammatic contraction: $\langle c_k^\dagger c_{k'-q'} \rangle \langle c_{k-q} c_{k'}^\dagger \rangle$. The propagator for the free field theory is $\langle c_k^\dagger c_{k'} \rangle = \delta_{kk'} f(k)$ where $f(k)$ is the Fermi function evaluated at ϵ_k . The above expression reduces to

$$\sum_k e^{i(\epsilon_k - \epsilon_{k-q})t} V_{kq} V_{k-q,-q} f(k) (1 - f(k-q)) \quad (\text{B6})$$

Taking the continuum limit in k and Fourier transforming in time gives the dynamical correlation function

$$\chi^{MF}(q, \omega) = \int \frac{dk}{2\pi} \delta(\omega + \epsilon_k - \epsilon_{k-q}) V_{kq} V_{k-q, -q} f(k) (1 - f(k - q)) \quad (\text{B7})$$

To lowest order in fermionic operators, the first non-

vanishing contribution to the Raman response χ^{MF} is a 4-spinon response. Using standard manipulations we find

$$\chi^{MF}(q, \omega) \propto \sum_{k_0} \frac{\sqrt{(2v_s \sin(q/2))^2 - \omega^2}}{(2v_s \sin(q/2))^2} f(k_0) (1 - f(k_0 - q)) \quad (\text{B8})$$

where the wavevector $k_0 \in [-\pi, \pi]$ satisfies conservation of energy $\omega + \epsilon_{k_0} - \epsilon_{k_0 - q} = 0$ (i.e. at low frequencies it is $\pm 2k_F$). For $q = \pi$, we recover Eq. (7).

Appendix C: Linearized Mean Field Theory

Here again for completeness we walk an interested reader through the standard manipulations for computing the low energy fermion response function Eq. (B7). At low energies, the response is proportional to the density-density correlation function given by

$$\chi^{MF}(q, \omega) \approx W(q, \omega) \chi''_{\rho\rho}(q, \omega) \quad (\text{C1})$$

where W is an overall function W of q and ω and the density-density correlation function is

$$\chi''_{\rho\rho}(q, \omega) = \int dt e^{i\omega t} \langle \rho_q^\dagger(t) \rho_q(0) \rangle_0 \quad (\text{C2})$$

with $\rho_q = \sum_k c_k^\dagger c_{k+q}$ and $\rho_q^\dagger = \rho_{-q}$.

In the limit where $V_{kq} = 1$, Eq. (B7) is exactly the density-density correlation function. We thus first inspect the low energy response of Eq. (C2). In this limit, the dispersion near the Fermi points is given by $\epsilon_k \approx \pm v k$. For ω small, energy conservation imposes $\epsilon_{k-q} \approx \epsilon_k$. Excitations at the same fermi point give $(\omega/v)\delta(\omega - v|q|)$, so we must look for excitations across both Fermi points. Suppose k is near one of the Fermi points, say $k = k_F + \delta k$ with $|\delta k|$ small. For $q = 2k_F + \delta q$ with $|\delta q|$ small, we have $k - q = -k_F + \delta k - \delta q$ near the left Fermi point. For these excitations, we have $\omega = \epsilon_{k-q} - \epsilon_k = -v(\delta k - \delta q) - (v)(\delta k) = -v(2\delta k - \delta q)$. Rearranging, we have $\delta k = \frac{1}{2}(\delta q - \omega/v)$ or $k = k_F + \frac{1}{2}(\delta q - \omega/v)$. Similarly, $k - q = -k_F + \frac{1}{2}(-\delta q - \omega/v)$. The Fermi functions place k below the right Fermi point ($|k| < k_F$) and $k - q$ above the left Fermi point ($|k - q| > k_F$). These constraints give $\delta q - \omega/v < 0$ and $-\delta q - \omega/v < 0$. Together, we have $\omega > v|\delta q| = v|q - 2k_F|$. A similar analysis of excitations from the left Fermi point to the right Fermi point gives $\omega > v|q + 2k_F|$.

Integration of Eq. (B7) over k yields a proportionality factor of the product of the vertices $V_{kq} V_{k-q, -q}$, with $k =$

$\pm \frac{1}{2}(q - \omega/v)$. The product of the vertices thus becomes an overall function of q and ω given by

$$W(q, \omega) = V_{\pm \frac{1}{2}(q - \omega/v), q} V_{\mp \frac{1}{2}(q + \omega/v), -q} \quad (\text{C3})$$

The vertex functions evaluate to an overall function W of q and ω . The low energy response of Eq. (B7) is given by

$$\chi^{MF}(q, \omega) \sim W(q, \omega) \chi''_{\rho\rho}(q, \omega) \quad (\text{C4})$$

where the low energy response of $\chi''_{\rho\rho}$ is

$$\chi''_{\rho\rho}(q, \omega) \sim \sum_{\pm} \Theta(\omega - v|q \pm 2k_F|) + (\omega/v)\delta(\omega - v|q|) \quad (\text{C5})$$

with Θ being the Heaviside step function. The low energy response of χ^{MF} thus follows the low energy response of $\chi''_{\rho\rho}$.

Appendix D: Bosonization

We incorporate interactions beyond mean field to capture the low energy Raman response of zigzag domain walls in bosonization. Recall the Luttinger liquid action [18] given by

$$S_{\text{Luttinger}} = \frac{1}{2\pi K} \int dx d\tau \left[\frac{1}{v_s} (\partial_\tau \phi)^2 + v_s (\partial_x \phi)^2 \right] \quad (\text{D1})$$

which is fully parameterized by the spinon velocity v_s and the Luttinger parameter K . This action describes the low energy physics of the 1D XXZ model. At $K = 1$, the theory corresponds to the U(1) point (isotropic XY model) whereas at $K = 1/2$ it corresponds to the SU(2) symmetric point (isotropic Heisenberg model). We note that in the $K \rightarrow 1$ limit, our mean field analysis becomes exact.

While the Luttinger parameter K generically depends on the applied magnetic field, in small magnetic fields we consider the case where K is not appreciably renormalized. At $h^z = 0$, the effective action of the system is precisely that of the Luttinger liquid. In applied magnetic

field ($h^z > 0$), however, the Luttinger parameter K is renormalized away from $K = 1/2$. As h^z approaches the saturation field $h_{sat} = 2J$, K approaches the free point $K = 1$ [29]. As previously shown, the singular magnetic field response of zigzag domain walls is observed at small magnetic fields near the critical field $h_c = \frac{1}{2}v_s(\pi/L_d)$ where L_d is the length of a zigzag domain. For such small fields we do not expect the Luttinger parameter to appreciably renormalize, and we may qualitatively understand the physics at $K = 1/2$ without renormalization.

In order to capture the effect of small applied magnetic fields, we track how the wavevector of the Fermi points shifts due to the chemical potential of fermionic spinons created by a nonzero magnetic field. Recall that bosonization is the low energy field theory at the Fermi points, but the location (momenta) of the Fermi points is an external parameter that does not appear within the bosonized theory. Explicitly,

$$\chi^{bos}(q, \omega, h^z) = \chi_{\rho\rho}(q - 2h^z/v_s, \omega) \quad (D2)$$

We capture the effect of domain walls by consider a Raman response at a shifted wavevector of $q = \pi \pm \pi/L_d$ with a zigzag domain length of L_d , or a distribution of domain sizes.

Appendix E: Effect of Zigzag Domain Walls on the Hamiltonian

In the main text we consider crystal domain walls in zigzag chains and the resulting Raman response. Our numerics take the limit where such domain walls do not appreciably modify the Hamiltonian nor the Raman operator. In a physical system, however, bonds with such defects would necessarily be modified in both the effective 1D Hamiltonian and in the Raman operator. Modifications in the Hamiltonian would manifest as changes in the spin exchange coupling due to any changes in the bond length. The relative orientation of these bonds with photon polarizations would also affect their bond strength in the Raman operator.

Even when domain walls appreciably modify the Hamiltonian or the Raman operator, we find no qualitative change in our conclusions. We may capture such changes directly in our numerics. When only spin exchange couplings in the Hamiltonian are modified, the magneto-Raman spectrum (Fig. 8, left) qualitatively reproduces the spectrum from the main text (Fig. 2). When both the Hamiltonian and the Raman operator are modified by zigzag domain walls, we again find the same qualitative spectral features (Fig. 8, right).

Local modifications to the Raman operator add disorder which can appear as background noise, but don't do much else. In particular, the qualitative features of the Raman response may still be captured by the most dominant Fourier mode q^* of the Raman operator by studying $\chi(q^*, \omega)$.

Changes to the Hamiltonian, however, are more subtle. We may consider two limiting cases where domain walls do or don't modify the Hamiltonian. In one limit, the Hamiltonian is not modified at all. In this case as discussed in the main text, we may approximate the Raman response by consider a Raman operator with a smoothed out bond profile which has nodes precisely at the defects. In the opposite limit, we may consider the case where domain walls do modify the Hamiltonian locally, and consider the 1D case (as in the current toy model) where such local perturbations are RG relevant and flow to infinite strength. The fixed point of the renormalization group flow takes the system to an open chain. This fragmented chains limit is discussed in the main text.

Appendix F: Linear Spin Wave Theory

In the main text, we demonstrated an anomalous, singular response to magnetic fields that may be observed by Raman scattering in phases without magnetic order, but we did not consider whether such a response could be measured in magnetically ordered phases. This begs the question as to whether or not the presence of magnetic order precludes the anomalous response.

Previously we employed a spinon parton construction of spin operators to compute the mean field Raman response. For magnetically ordered phases, however, spin excitations from the ground state are described by magnons. In this section, we compute the Raman response of R_q Eq. (11) using a magnon parton construction for the 1D Heisenberg Hamiltonian in applied field. We compute this response within linear spin-wave theory (LSWT) and only to lowest non-vanishing order in bosonic operators.

It is well known [21], however, that quantum fluctuations in 1D diverge and obstruct the precipitation of magnetic order. Nonetheless, we employ LSWT in order to gain intuition for how quasi-1D spin chains may behave in the presence of magnetic order mediated by interactions in 3D. We find that bosonic magnon excitations, unlike fermionic spinon excitations, lack the anomalous, singular magnetic field response we present in the main text. Whereas an applied magnetic field shifts the Fermi momentum of a spinon Fermi surface, and may tune gapped excitations to become gapless, bosonic magnon excitations do not experience such an effect. Indeed, for 1D magnons we find no similar anomalous magnetic field response that is probed by Raman scattering.

To begin, we first consider magnons in a ferromagnetic phase in applied magnetic field. We then consider the antiferromagnetic phase at zero applied field. In this case, we find the Raman response to be non-vanishing at the 4-magnon level. In applied field, however, the classical ground state of the antiferromagnet changes. At finite field, the Raman response then becomes non-vanishing at the 2-magnon level and mimics the dynamical structure factor probed by neutron scattering. In all cases,

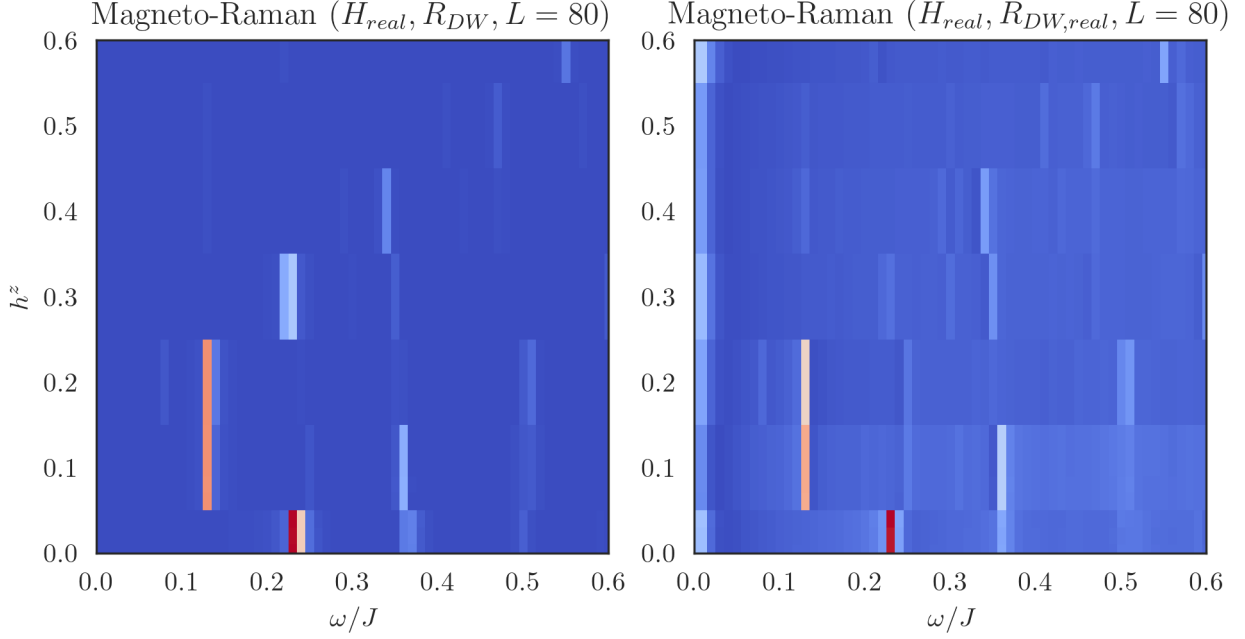


FIG. 8. Numerically computed inelastic magneto-Raman spectra for finite sized systems ($L=80$ sites) where zigzag domain walls modify the Hamiltonian (color scale is identical to Fig. 2). In both cases, the system hosts zigzag domain walls on lattice sites $j_1=26$ and $j_2=54$. The Hamiltonian is $H_{\text{real}} = \sum_{j=1}^L J_j \mathbf{S}_j \cdot \mathbf{S}_{j+1}$ with $J_j = 1$ for $j \neq j_1, j_2$ and $J_j = 0.3$ for $j = j_1, j_2$. The Raman operator R_{DW} is the same as Fig. 2, while the Raman operator $R_{DW,\text{real}}$ is defined similarly to H_{real} . Explicitly $R_{DW,\text{real}} = \sum_{j=1}^L g_j \mathbf{S}_j \cdot \mathbf{S}_{j+1}$ with $g_j = \frac{1}{2}(1 + (-1)^j)$ for $j < j_1$ and $j > j_2$, $g_j = \frac{1}{2}(1 + (-1)^{j+1})$ for $j_1 < j < j_2$, and $g_j = 0.5$ for $j = j_1, j_2$. (Left) Magneto-Raman spectrum when zigzag domain walls only modify the Hamiltonian. (Right) Magneto-Raman spectrum when zigzag domain walls modify both the Hamiltonian and the Raman operator. In both cases, we obtain the same qualitative features as Fig. 2.

however, the magnetic field dependence of the Raman response lacks the anomaly we find for free spinons in the main text.

1. Ferromagnetic Phase

For the spin- S ferromagnetic Heisenberg Hamiltonian ($J < 0$) with periodic boundary conditions, we may transform spin operators to bosonic magnon operators via the Holstein-Primakoff transformation Eq. (F1)

$$S_i^z = S - a_i^\dagger a_i, \quad S_i^- = a_i^\dagger \sqrt{2S - a_i^\dagger a_i}, \quad S_i^+ = (S_i^-)^\dagger \quad (\text{F1})$$

with $[a_i, a_j^\dagger] = \delta_{ij}$. Within LSWT, we expand in powers of $(a_i^\dagger a_i/2S)$ and keep bosonic operators up to quadratic order. For the present case, LSWT yields a free bosonic

Hamiltonian Eq. (F2) after a Fourier transform

$$H_{FM} = \sum_k \epsilon_k a_k^\dagger a_k, \quad \epsilon_k = 2|J|S(1 - \cos(k)) + h^z \quad (\text{F2})$$

The Raman operator R_q within LSWT reads

$$R_q = \sum_k \Gamma_{kq} a_k^\dagger a_{k+q} \quad (\text{F3})$$

with the vertex given by Eq. (F4).

$$\Gamma_{kq} = S(e^{-i(k+q)} + e^{ik} - 1 - e^{-iq}) \quad (\text{F4})$$

The Raman operator R_q is thus a magnon density excitation at momentum q . To lowest order in bosonic operators, the first non-vanishing contribution to the Raman response χ^{FM} is a 4-magnon response (at finite T).

We perform calculations analogous to the main text and find

$$\chi^{FM}(q, \omega) = \sum_{k_0} \frac{\Gamma_{k_0, q} \Gamma_{k_0+q, -q} n(k_0)(1 + n(k_0 + q))}{\sqrt{(4JS \sin(q/2))^2 - \omega^2}} \quad (\text{F5})$$

where $k_0 \in [-\pi, \pi]$ satisfies $\omega + \epsilon_{k_0} - \epsilon_{k_0+q} = 0$, and Bose

functions are given by $n(k) = (e^{\beta \epsilon_k} - 1)^{-1}$.

At $T = 0$, however, the ground state is the magnon vacuum. The Raman response at this order vanishes since $R_q(t = 0)$ annihilates the ground state. As such we conclude the magnon-Raman response of R_q vanishes within LSWT for the ferromagnetic phase.

2. Antiferromagnetic Phase ($h = 0$)

At zero magnetic field, the classical ground state of the antiferromagnetic phase is the Néel state. To perform LSWT, we first apply rotate spins by π about the x -axis on every other lattice site. Under this transformation, spins on one sublattice transform like $S_j^z \mapsto -S_j^z$ and $S_j^\pm \mapsto S_j^\mp$. Under this rotation, Holstein-Primakoff bosons are the appropriate fluctuations about the classical antiferromagnetic ground state. The Heisenberg Hamiltonian after this sublattice rotation is given by Eq. (F6).

$$H = J \sum_j \frac{1}{2} (S_j^- S_{j+1}^- + S_j^+ S_{j+1}^+) - S_j^z S_{j+1}^z \quad (\text{F6})$$

Keeping only quadratic terms in Holstein-Primakoff bosons and performing a Fourier transform, the Hamiltonian becomes (up to an overall constant)

$$H = 2JS \sum_k a_k^\dagger a_k + \frac{1}{2} \gamma_k (a_k a_{-k} + a_k^\dagger a_{-k}^\dagger) \quad (\text{F7})$$

where $\gamma_k = \cos(k)$ is the sum of lattice harmonics in 1D. While the Hamiltonian is not diagonal in these bosonic operators, we may employ a Bogoliubov transform to diagonalize it

$$\begin{pmatrix} b_k \\ b_{-k}^\dagger \end{pmatrix} = \begin{pmatrix} \cosh \phi_k & \sinh \phi_k \\ \sinh \phi_k & \cosh \phi_k \end{pmatrix} \begin{pmatrix} a_k \\ a_{-k}^\dagger \end{pmatrix} \quad (\text{F8})$$

The Hamiltonian is diagonalized for $\gamma_k = \tanh 2\phi_k$ and reads

$$H = \sum_k \epsilon_k (b_k^\dagger b_k + 1/2), \quad \epsilon_k = 2JS |\sin(k)| \quad (\text{F9})$$

with $[b_k, b_{k'}^\dagger] = \delta_{kk'}$.

The Raman operator R_q within LSWT may be similarly constructed. We find

$$R_q = \sum_k \Psi_k^\dagger M_{kq} \Psi_{k+q}, \quad \Psi_k = \begin{pmatrix} b_k \\ b_{-k}^\dagger \end{pmatrix} \quad (\text{F10})$$

with the vertex given by Eq. (F11). In the expression, σ^0, σ^1 denote the 2×2 identity and x Pauli matrices respectively.

$$M_{kq} = \sigma^0 |\csc(k)| \left[\frac{1}{2} (1 + e^{iq}) - e^{-i(k+q)} \cos(k) \right] + \sigma^1 |\csc(k)| \left[e^{-i(k+q)} - \frac{1}{2} (1 + e^{iq}) \cos(k) \right] \quad (\text{F11})$$

Time evolution of R_q in this form is straightforward and given by

$$R_q(t) = \sum_k \Psi_k^\dagger U_k^\dagger(t) M_{kq} U_{k+q}(t) \Psi_{k+q} \quad (\text{F12})$$

where $U_k(t) = \exp(-i\sigma^3 \epsilon_k t)$ and σ^3 is the usual z Pauli

matrix.

The Raman response may then be evaluated diagrammatically. At $T = 0$, the ground state of the system is the magnon vacuum. Hence only correlations of the form $\langle a_{k_1}(t) a_{k_2}(t) a_{k_3}^\dagger(0) a_{k_4}^\dagger(0) \rangle$ contribute to a finite response. In total, we find a finite response Eq. (F13) which follows the magnon dispersion.

$$\chi^{AFM}(q, \omega) = \frac{1}{\sqrt{(4JS \cos(q/2))^2 - \omega^2}} \sum_{k_0 \in [0, \pi], k_0 \in [-\pi, 0]} (M_{k_0, q})_{21} [(M_{-k_0, -q})_{12} + (M_{k_0+q, -q})_{12}] \quad (\text{F13})$$

In the response Eq. (F13), the sum over $k_0 \in [0, \pi], [-\pi, 0]$ is taken over the right/left halves of the first Brillouin zone, with k_0 satisfying $\omega - (\epsilon_{k_0} + \epsilon_{k_0+q}) = 0$, and $(M_{kq})_{ij}$ denote the ij -th matrix element of the vertex expressed in Eq. (F11).

3. Antiferromagnetic Phase ($h > 0$)

While at zero magnetic field, the classical ground state of the antiferromagnetic phase is the Néel state, in applied magnetic field this is not the case. Classical spins cant by an angle θ_c to align with the applied field. Following [30–32], we allow spins to cant by an angle θ about the \hat{y} axis away from the Néel state. The classical ground state energy is minimized for $\sin \theta_c = h^z/4JS$.

Within LSWT, the Hamiltonian no longer conserves magnon number. Indeed, we find

$$H = \sum_k A_k a_k^\dagger a_k - \frac{B_k}{2} (a_k a_{-k} + a_k^\dagger a_{-k}^\dagger) \quad (\text{F14})$$

with $A_k = 2JS(1 + \sin^2(\theta_c)\gamma_k)$, $B_k = 2JS \cos^2(\theta_c)\gamma_k$, and $\gamma_k = \cos(k)$ is the sum of lattice harmonics for the

1D spin chain. Note, for $h = 0 \implies \theta_c = 0$, the coefficients A_k, B_k are precisely those found in the previous section. We may again employ a Bogoliubov transformation to diagonalize H . In this case, the Hamiltonian is diagonalized for $\tanh(2\phi_k) = -B_k/A_k$. Then

$$H = \sum_k \epsilon_k (b_k^\dagger b_k + 1/2) \quad (\text{F15})$$

where

$$\epsilon_k = 2JS \sqrt{(1 + \gamma_k)(1 - \cos(2\theta_c)\gamma_k)} \quad (\text{F16})$$

For $\theta = \theta_c$, the linear magnon terms in H vanish identically. For the Raman operator R_q , however, this is not the case. Indeed, to lowest order in Bogoliubov magnons b_k , we find

$$R_q = \sqrt{\frac{S^3}{2}} \sin(2\theta_c) (1 + e^{-iq}) e^{\phi - q + \pi} (b_{q+\pi} + b_{-(q+\pi)}^\dagger) \quad (\text{F17})$$

Physically, R_q creates a single magnon excitation at $\pm(q + \pi)$.

The Raman response χ^{AFM} of R_q to lowest order is a 2-magnon response. At this order, we find

$$\chi^{AFM}(q, \omega) = 2JS^4 \sin(2\theta_c) \sin^2(q) \frac{\delta(\omega - \epsilon_{q+\pi})}{\omega} \quad (\text{F18})$$

At $h^z = 0$, $\theta_c = 0$ and so this contribution of the response vanish.

We may follow a similar procedure as in the ferromagnetic phase to compute the 4-magnon response. We find the response qualitatively follows the $h^z \rightarrow 0^+$ limit of the 2-magnon response, and so we omit the calculation here.

Appendix G: Raman response of geometric defects (small amplitude bond variation)

In this section we will consider small amplitude bond variations in a zigzag chain and determine the subsequent Raman response. We will restrict ourselves to the nearest neighbor Heisenberg Hamiltonian $H = J \sum_j \mathbf{S}_j \cdot \mathbf{S}_{j+1}$. Suppose the bond angle generically depends on the lattice site

$$\theta_j = \theta_0 + \epsilon f_j \quad (\text{G1})$$

where θ_0 is the equilibrium bond angle and $\epsilon \ll 1$. We let the variation f in the bond angle be arbitrary.

$$R = \sum_j (\mathbf{e}_i \hat{\mathbf{e}}_i \cdot \mathbf{r}_j) (\hat{\mathbf{e}}_s \cdot \mathbf{r}_j) (\mathbf{S}_j \cdot \mathbf{S}_{j+1}) \quad (\text{G2})$$

where \mathbf{r}_j is the bond vector pointing from site j to site $j + 1$. For a zigzag chain formed from isosceles triangles, we have

$$\mathbf{r}_j = \begin{pmatrix} \cos(\theta_j) \\ (-1)^j \sin(\theta_j) \end{pmatrix}, \quad \hat{\mathbf{e}}_{i,s} = \begin{pmatrix} \cos \theta_{i,s} \\ \sin \theta_{i,s} \end{pmatrix} \quad (\text{G3})$$

Thus

$$(\hat{\mathbf{e}}_i \cdot \mathbf{r}_j) (\hat{\mathbf{e}}_s \cdot \mathbf{r}_j) = (\cos \theta_i \cos \theta_s \cos^2 \theta_j + \sin \theta_i \sin \theta_s \sin^2 \theta_j) + (-1)^j \sin(\theta_i + \theta_s) \cos \theta_j \sin \theta_j \quad (\text{G4})$$

When $\theta_i + \theta_s = \frac{\pi}{2}$, to order $O(\epsilon^2)$ we find (up to spectral

equivalence)

$$(\hat{\mathbf{e}}_i \cdot \mathbf{r}_j)(\hat{\mathbf{e}}_s \cdot \mathbf{r}_j) \rightarrow (-1)^j \left[\frac{1}{2} \sin(2\theta_0) + \epsilon f(j) \cos(2\theta_0) - (\epsilon f(j))^2 \sin(2\theta_0) \right] \quad (\text{G5})$$

We next define the following operators

$$R_q = \sum_j e^{iqj} (\mathbf{S}_j \cdot \mathbf{S}_{j+1}) \quad (\text{G6})$$

$$R[f] = \sum_j (-1)^j f_j (\mathbf{S}_j \cdot \mathbf{S}_{j+1}) = \sum_q \tilde{f}_{q+\pi} R_q \quad (\text{G7})$$

where \tilde{f}_q is the Fourier transform of f_j . The Raman operator then reads

$$R = \frac{1}{2} \sin(2\theta_0) R_\pi + \epsilon \cos(2\theta_0) \sum_q \tilde{f}_{q+\pi} R_q + \epsilon^2 (-\sin(2\theta_0)) \sum_q (\tilde{f}^2)_{q+\pi} R_q \quad (\text{G8})$$

We then compute the Raman correlator $\langle R_q(t) R_{q'}(0) \rangle$ to find the Raman response $\chi(q, \omega)$ as before. The Raman

response with small angle variations is then readily found to be $I(\omega) = I_0(\omega) + \epsilon I_1(\omega) + \epsilon^2 I_2(\omega) + O(\epsilon^3)$ where each intensity contribution is given by

$$I_0(\omega) = \frac{1}{4} \sin^2(2\theta_0) \chi(\pi, \omega) \quad (\text{G9})$$

$$\begin{aligned} I_1(\omega) &= \sin(2\theta_0) \cos(2\theta_0) \sum_q \tilde{f}_{q+\pi} \int dt e^{i\omega t} \langle R_\pi(t) R_q(0) \rangle \\ &= \sin(2\theta_0) \cos(2\theta_0) \tilde{f}_0 \chi(\pi, \omega) \end{aligned} \quad (\text{G10})$$

$$\begin{aligned} I_2(\omega) &= -\sin^2(2\theta_0) \sum_q (\tilde{f}^2)_{q+\pi} \int dt e^{i\omega t} \langle R_\pi(t) R_q(0) \rangle + \cos^2(2\theta_0) \sum_{qq'} \tilde{f}_{q+\pi} \tilde{f}_{q'+\pi} \int dt e^{i\omega t} \langle R_q(t) R_{q'}(0) \rangle \\ &= -\sin^2(2\theta_0) (\tilde{f}^2)_0 \chi(\pi, \omega) + \cos^2(2\theta_0) \sum_q |\tilde{f}_q|^2 \chi(q + \pi, \omega) \end{aligned} \quad (\text{G11})$$

Rearranging, we have

$$I(\omega) = \sin(2\theta_0) \left(\frac{1}{2} \sin(2\theta_0) + \epsilon \cos(2\theta_0) \tilde{f}_0 - \epsilon^2 \sin(2\theta_0) (\tilde{f}^2)_0 \right) \chi(\pi, \omega) + \epsilon^2 \cos(2\theta_0) \sum_q |\tilde{f}_q|^2 \chi(q + \pi, \omega) \quad (\text{G12})$$

Appendix H: Mathematical treatment of Poisson distributions

The power spectrum of the Raman operator bond profile can be computed exactly when zigzag domain sizes are Poisson distributed – an unphysical limit but worth discussing for mathematical completeness. Consider a random telegraph signal generated by a Poisson point

process.

Let g_j take on values of ± 1 . Suppose the probability of observing m zigzag domains with positive parity over a distance x is given by

$$p(m, x) = \frac{(\mu x)^m}{m!} e^{-\mu x} \quad (\text{H1})$$

with μ the mean number of positive parity domains per unit length. We may then compute the autocorrelation

function $\phi_x(g) = g_j g_{j+x}$. The autocorrelation function $\phi_x(g)$ is +1 if the number of domains with particular parity found in the interval of lattice sites $(j, j+x)$ is even. Similarly $\phi_x(g) = -1$ if the number is odd. Hence the autocorrelation is given by

$$\phi_x(g) = \sum_{k=0}^{\infty} p(2k, x) - p(2k+1, x) = e^{-2\mu x} \quad (\text{H2})$$

The power spectrum of g_j is then the Fourier transform of $\phi_x(g)$ by the Wiener-Khinchin theorem. This is a Lorentzian centered at $q = 0$ whose full-width at half-maximum scales linearly with μ^{-1} .

$$|g_q|^2 \propto \frac{1/\mu}{(1 + (q/2\mu)^2)} \quad (\text{H3})$$

-
- [1] Y. Ran, Y. Zhang, and A. Vishwanath, One-dimensional topologically protected modes in topological insulators with lattice dislocations, *Nature Physics* **5**, 298 (2009).
- [2] M. Azuma, Y. Fujishiro, M. Takano, M. Nohara, and H. Takagi, Switching of the gapped singlet spin-liquid state to an antiferromagnetically ordered state in $\text{Sr}(\text{Cu}_{1-x}\text{Zn}_x)_2\text{O}_3$, *Phys. Rev. B* **55**, R8658 (1997).
- [3] A. J. Willans, J. T. Chalker, and R. Moessner, Disorder in a quantum spin liquid: Flux binding and local moment formation, *Phys. Rev. Lett.* **104**, 237203 (2010).
- [4] W.-H. Kao, J. Knolle, G. B. Halász, R. Moessner, and N. B. Perkins, Vacancy-induced low-energy density of states in the kitaev spin liquid, *Phys. Rev. X* **11**, 011034 (2021).
- [5] A. Eckmann, A. Felten, A. Mishchenko, L. Britnell, R. Krupke, K. S. Novoselov, and C. Casiraghi, Probing the nature of defects in graphene by raman spectroscopy, *Nano Letters* **12**, 3925 (2012).
- [6] I. Kimchi, A. Nahum, and T. Senthil, Valence bonds in random quantum magnets: Theory and application to YbMgGaO_4 , *Phys. Rev. X* **8**, 031028 (2018).
- [7] M. Hase, H. Kuroe, K. Ozawa, O. Suzuki, H. Kitazawa, G. Kido, and T. Sekine, Magnetic properties of $\text{Rb}_2\text{Cu}_2\text{Mo}_3\text{O}_{12}$ including a one-dimensional spin-1/2 heisenberg system with ferromagnetic first-nearest-neighbor and antiferromagnetic second-nearest-neighbor exchange interactions, *Phys. Rev. B* **70**, 104426 (2004).
- [8] S. Hayashida, D. Blosser, K. Y. Povarov, Z. Yan, S. Gvasaliya, A. N. Ponomaryov, S. A. Zvyagin, and A. Zheludev, One- and three-dimensional quantum phase transitions and anisotropy in $\text{Rb}_2\text{Cu}_2\text{Mo}_3\text{O}_{12}$, *Phys. Rev. B* **100**, 134427 (2019).
- [9] S. Selzer, Y. Shemerliuk, B. Büchner, and S. Aswartham, Crystal growth of the quasi-2d quaternary compound AgCrP_2S_6 by chemical vapor transport, *Crystals* **11**, 10.3390/cryst11050500 (2021).
- [10] H. Mutka, C. Payen, and P. Molinié, One-dimensional heisenberg antiferromagnet with spin $s = 3/2$. experiments on AgCrP_2S_6 , *Europhysics Letters* **21**, 623 (1993).
- [11] D. C. Dender, P. R. Hammar, D. H. Reich, C. Broholm, and G. Aeppli, Direct observation of field-induced incommensurate fluctuations in a one-dimensional $S = 1/2$ antiferromagnet, *Phys. Rev. Lett.* **79**, 1750 (1997).
- [12] Y. Yang, M. Li, I. Rousochatzakis, and N. B. Perkins, Non-loudon-fleury raman scattering in spin-orbit coupled mott insulators, *Phys. Rev. B* **104**, 144412 (2021).
- [13] I. Affleck and M. Oshikawa, Field-induced gap in Cu benzoate and other $s = \frac{1}{2}$ antiferromagnetic chains, *Phys. Rev. B* **60**, 1038 (1999).
- [14] W. Brenig, Raman scattering from frustrated quantum spin chains, *Phys. Rev. B* **56**, 2551 (1997).
- [15] P. A. Fleury and R. Loudon, Scattering of Light by One- and Two-Magnon Excitations, *Physical Review* **166**, 514 (1968).
- [16] M. Sato, H. Katsura, and N. Nagaosa, Theory of raman scattering in one-dimensional quantum spin- $\frac{1}{2}$ antiferromagnets, *Phys. Rev. Lett.* **108**, 237401 (2012).
- [17] J. des Cloizeaux and J. J. Pearson, Spin-wave spectrum of the antiferromagnetic linear chain, *Phys. Rev.* **128**, 2131 (1962).
- [18] T. Giamarchi, *Quantum physics in one dimension*, The international series of monographs on physics No. 121 (Clarendon ; Oxford University Press, Oxford : New York, 2004).
- [19] S. Eggert and I. Affleck, Magnetic impurities in half-integer-spin Heisenberg antiferromagnetic chains, *Physical Review B* **46**, 10866 (1992).
- [20] Y. Imry and S.-k. Ma, Random-field instability of the ordered state of continuous symmetry, *Phys. Rev. Lett.* **35**, 1399 (1975).
- [21] N. D. Mermin and H. Wagner, Absence of ferromagnetism or antiferromagnetism in one- or two-dimensional isotropic heisenberg models, *Phys. Rev. Lett.* **17**, 1133 (1966).
- [22] E. S. Sørensen and I. Affleck, Large-scale numerical evidence for bose condensation in the $s=1$ antiferromagnetic chain in a strong field, *Phys. Rev. Lett.* **71**, 1633 (1993).
- [23] I. Affleck, Bose condensation in quasi-one-dimensional antiferromagnets in strong fields, *Physical Review B* **43**, 3215 (1991).
- [24] N. Perkins and W. Brenig, Raman scattering in a heisenberg $s = \frac{1}{2}$ antiferromagnet on the triangular lattice, *Phys. Rev. B* **77**, 174412 (2008).
- [25] J. Knolle, G.-W. Chern, D. L. Kovrizhin, R. Moessner, and N. B. Perkins, Raman scattering signatures of kitaev spin liquids in A_2IrO_3 iridates with $a = \text{Na}$ or Li , *Phys. Rev. Lett.* **113**, 187201 (2014).
- [26] B. Perreault, J. Knolle, N. B. Perkins, and F. J. Burnell, Theory of raman response in three-dimensional kitaev spin liquids: Application to β - and γ - Li_2IrO_3 compounds, *Phys. Rev. B* **92**, 094439 (2015).
- [27] J. Hauschild and F. Pollmann, Efficient numerical simulations with Tensor Networks: Tensor Network Python (TeNPy), *SciPost Phys. Lect. Notes* , 5 (2018).
- [28] T. Barthel and Y. Zhang, Optimized lie-trotter-suzuki decompositions for two and three non-commuting terms, *Annals of Physics* **418**, 168165 (2020).
- [29] D. C. Cabra and P. Pujol, Field-theoretical methods in quantum magnetism, in *Quantum Magnetism*, Lecture Notes in Physics, edited by U. Schollwöck, J. Richter, D. J. J. Farnell, and R. F. Bishop (Springer, Berlin, Heidelberg, 2004) pp. 253–305.

- [30] M. E. Zhitomirsky and T. Nikuni, Magnetization curve of a square-lattice Heisenberg antiferromagnet, *Physical Review B* **57**, 5013 (1998).
- [31] M. E. Zhitomirsky and A. L. Chernyshev, Instability of Antiferromagnetic Magnons in Strong Fields, *Physical Review Letters* **82**, 4536 (1999).
- [32] O. F. Syljuåsen, Numerical evidence for unstable magnons at high fields in the Heisenberg antiferromagnet on the square lattice, *Physical Review B* **78**, 180413 (2008).
- [33] M. McGinley, M. Fava, and S. A. Parameswaran, Signatures of fractional statistics in nonlinear pump-probe spectroscopy (2022).
- [34] F. Harper, R. Roy, M. S. Rudner, and S. Sondhi, Topology and Broken Symmetry in Floquet Systems, *Annual Review of Condensed Matter Physics* **11**, 345 (2020).